

A Finite Element Based Methodology for Inverse Problem of Determining Contact Forces Using Measured Displacements

Jiangtao Song and Randy J Gu

Department of Mechanical Engineering, Oakland University, Rochester, Michigan 48309, USA, gu@oakland.edu

Abstract

The identification of contact forces applied on a solid body or structure is a special case of a general class of inverse problems. This problem is very complicated, especially when there is insufficient boundary information in the region where the contact forces need to be identified. In this paper, the unknown loads or contact forces are identified by reconstructing the finite element formula and minimizing the criterion function derived as the sum of squares of the differences between measurements and numerical results of the finite element method. A detail description of the formulation, analysis and solution of the inverse problems are given. Tikhonov-Phillips regularization technique is employed to reduce the influence of the measurement noise. Three examples are chosen to demonstrate the accuracy of the numerical algorithm.

Keywords: inverse problem; contact force; finite element; regularization

1. Introduction

Contact problems exist in many engineering applications such as metal forming, fastening and joining, mechanism, etc. The analysis of contact problems of elastic bodies has attracted considerable concern in many industries and researchers. Much of the difficulty of such analysis lies in the undetermined boundary locations between the contact and non-contact regions and the unknown contact forces. Generally speaking, we do not know the actual regions of contact and the stress and displacements on the contacting surface prior to the solution of the problem. These unknowns associated with any contact problem render the resulting problem nonlinear. Depending on the loads, material, boundary conditions, and other factors, surfaces can come into and go out of contact with each other in a largely unpredictable manner. Hence, analytical solutions are obtained for very few of relatively simple problems. As a result, numerical procedures and simplified models are always invariably employed to simulate these contact problems.

Over the past decades, researchers have developed some theories and experimental as well as numerical methods to solve the contact problems. Some of the numerical methods have also been implemented for engineering design and applications in commercial codes such as ANSYS [1] and ABAQUS [2]. These codes have been used to solve common contact problems in the industry where the contacting objects are properly supported. The early work of Hertz [3], known as Hertzian contact theory, showed a relationship for determining the contact pressure distribution and contact radius of a rigid plane while in contact with an elastic sphere or cylinder under an applied load. For general kind of contact problems, the two widely used procedures to solve them are the Lagrange's multiplier method and the penalty function method [4]. Both these methods operate on the variational or weighted residual formulation of the problem under consideration. In the Lagrange's multiplier method, an additional variable called Lagrange's multiplier is introduced and the variation of the modified functional is set to zero. Thus, the equilibrium equations without a constraint are amended with an additional equation that embodies the constraint condition. This method is suitable when large displacements are present, so that nodes in the contactor that are not directly opposite a node in the target, at any given stage in the solution, can still be treated. In the penalty method, a large constant called penalty number multiplying the constraint function is introduced to amend the functional. For problems involving inequality constraints, singularity function, such as step function, may be introduced in the penalty function. In this approach, the constraint equations are only approximately satisfied. Most recently, Gu *et al.* [5] developed a modified penalty method in which the constant penalty number is replaced with a penalty variable. The penalty variable method is developed to solve the quasi-static problem involving objects with inadequate support at the start of the analysis that could not otherwise be solved using traditional penalty method and many existing finite element codes.

Research in solving contact problems using finite element method has been active in the past three decades. Campos *et al.* [6] presented a numerical analysis of frictional contact problems involving linearly elastic objects subject to both known and unknown contact pressures by finite element method. Penalized function was used to enforce the contact condition between the contacting objects. Oden and Kikuchi [7] showed various variational formulations of problems with equality and inequality constraints using Lagrange multiplier and penalty function methods. Yagawa and Hirayama [8] presented a finite element method for contact problems in fracture mechanics using penalty function method. Chen and Tsai [9] developed a finite element method for elastodynamic sliding contact problems with friction using Lagrange multiplier method. Bathe and Chaudhary presented a solution procedure for the planar contact problems under large deformation [10], where Lagrange multiplier method is used to account for the contact conditions. Gu [11], [12], [13] used the moving finite element analysis technique to examine the contact problems of elastic beams, including bending of beams on stationary rigid barriers [11] and indentation of beams subjected to a descending rigid punch [12], and two-dimensional elastic contact problems [13] with absence of slipping and friction between the contact objects. The interface equation, which is extracted by application of principle of minimum potential energy, was used to determine the unknown location of the marginal node separating the contact and non-contact regions. Fuehne and Engblom [14] used penalty function method for computing stresses near debonds in laminated composite structures for a problem with equality constraints. Upon assessing the stability and performance of several existing contact algorithms for flexible object contact problems, El-Abbasi and Bathe [15] developed a new algorithm that satisfies both the inf-sup and contact patch conditions. As demonstrated, the new segment-to-segment algorithm is proved to be stable and maintains quadratic convergence using either linear or quadratic contact elements.

Whilst the approaches in the work mentioned above are different, direct method is used to solve the contact problems. That is, using the given external forces to determine the deformation, contact domain and stress within the contact bodies. However, if the applied forces are unknown, how to identify the unknown contact or applied forces on a solid body or structure is a special case of inverse problems. Inverse problem of identification of unknown contact forces closely related to boundary measurements, such as displacement or strain fields on the boundary. Strains and displacements can be measured directly, e.g. using strain gauges. In manufacturing factory, in order to assess the surface quality of the parts, coordinate measurement machines (CMMs) are often employed to scan the parts to obtain measurement data. The data are then fitted to the nominal model to determine the surface quality of the product [17]. Such experimental techniques yield rich experimental data and are therefore well suited to identification problems, especially for the accessible boundary. In particular, recent optical techniques now allow us to measure displacement fields or in-plane strain fields on the boundary [18]. Gu [19] developed a numerical algorithm to determine the contact pressure between flexible objects using the measured friction forces. A set of narrow strips were placed between the contacting object and a rigid plane. The orientations of the strips were varied to emulating the technique commonly found in computerized tomography. By pulling the strips, a large set of forces were collected and used to reconstruct the contact pressure.

In this paper, the unknown loads or contact forces are identified by minimizing an objective function derived as the L_2 -norm of the differences between the measurements and the numerical results from a finite element method. A detail description of the formulation, analysis and solution of the inverse problems are given in the presentation. Tikhonov-Phillips regularization technique is used to reduce the influence of the noise embedded in the measurements. The calculation examples indicate that the present inverse method is a very useful tool for engineers to determine the contact forces, contact zones and deformed configurations of the contact objects based on the measured displacements.

2. Finite Element Procedure

Consider an isotropic, homogeneous, linear elastic body Ω with boundary conditions as shown in Figure 1, Γ_1 is the boundary with zero displacement, Γ_2 is the boundary where measured displacements are given, Γ_3 is the boundary with unknown contact forces \mathbf{F}_c and unknown contact deformation or displacements, and Γ_4 is the boundary where there are known applied forces $\bar{\mathbf{F}}_a$ and the other free surface except those mentioned above. The displacements on boundary Γ_4 are also unknown.

Let's recall the general form of static finite element system, which is

$$\mathbf{K}\mathbf{U} = \mathbf{F}. \quad (1)$$

where \mathbf{K} is the stiffness matrix of the system, \mathbf{U} is the nodal displacement vector, and \mathbf{F} is the vector of nodal forces.

According to the classification of the boundary above, we may easily reconstruct the finite element equation in the following form:

$$\begin{bmatrix} \mathbf{K}_{11} & \mathbf{K}_{12} & \mathbf{K}_{13} & \mathbf{K}_{14} \\ \mathbf{K}_{21} & \mathbf{K}_{22} & \mathbf{K}_{23} & \mathbf{K}_{24} \\ \mathbf{K}_{31} & \mathbf{K}_{32} & \mathbf{K}_{33} & \mathbf{K}_{34} \\ \mathbf{K}_{41} & \mathbf{K}_{42} & \mathbf{K}_{43} & \mathbf{K}_{44} \end{bmatrix} \begin{Bmatrix} \bar{\mathbf{U}}_1 \\ \mathbf{U}_2 \\ \mathbf{U}_3 \\ \mathbf{U}_4 \end{Bmatrix} = \begin{Bmatrix} \mathbf{F}_1 \\ \bar{\mathbf{F}}_2 \\ \mathbf{F}_c \\ \bar{\mathbf{F}}_a \end{Bmatrix}, \quad (2)$$

where

\mathbf{K}_{ij} = the sub-stiffness matrix;

\mathbf{F}_1 = the vector of reaction forces on the boundary Γ_1 ;

$\bar{\mathbf{F}}_2$ = the vector of forces on the boundary Γ_2 with measured displacements, usually, there is no forces on the measured boundary;

\mathbf{F}_c = the vector of unknown reaction or contact forces on the boundary Γ_3 ;

$\bar{\mathbf{F}}_a$ = the vector of known applied forces on the boundary Γ_4 , other free surfaces and internal nodes;

$\bar{\mathbf{U}}_1$ = known displacements on constrained boundary Γ_1 ;

\mathbf{U}_2 = measured displacements on free boundary Γ_2 ;

\mathbf{U}_3 = unknown displacements on contact boundary Γ_3 ;

\mathbf{U}_4 = unknown displacements on (a) boundary Γ_4 with known applied force $\bar{\mathbf{F}}_a$, (b) the free surface with no applied force and (c) the internal nodes where net force is zero.

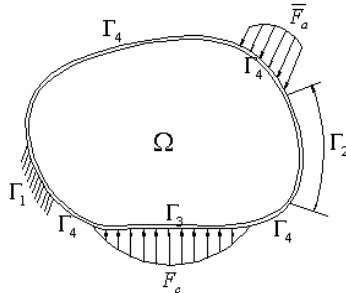


Figure 1. A general contact model for inverse analysis.

In the structure stiffness equation (2), the stiffness matrix is singular and no unique solution for the displacement is possible if the structure is unsupported. Therefore, the boundary conditions are needed to apply to the structure stiffness equations. Here, we assume that all displacements on boundary Γ_1 are zero, i.e. $\bar{\mathbf{U}}_1 = 0$. After applying this condition to the system matrix and vector in equation (2), the reduced FEA equation becomes

$$\begin{bmatrix} \mathbf{K}_{22} & \mathbf{K}_{23} & \mathbf{K}_{24} \\ \mathbf{K}_{32} & \mathbf{K}_{33} & \mathbf{K}_{34} \\ \mathbf{K}_{42} & \mathbf{K}_{43} & \mathbf{K}_{44} \end{bmatrix} \begin{Bmatrix} \mathbf{U}_2 \\ \mathbf{U}_3 \\ \mathbf{U}_4 \end{Bmatrix} = \begin{Bmatrix} \bar{\mathbf{F}}_2 \\ \mathbf{F}_c \\ \bar{\mathbf{F}}_a \end{Bmatrix}. \quad (3)$$

Our purpose is to calculate the unknown applied or contact forces \mathbf{F}_c with given measurements \mathbf{U}_2 . In the following section, we will elaborate on how to establish a relation between the unknown contact forces and the measured displacements. First, let us look at the third equation in (3):

$$\mathbf{K}_{42}\mathbf{U}_2 + \mathbf{K}_{43}\mathbf{U}_3 + \mathbf{K}_{44}\mathbf{U}_4 = \bar{\mathbf{F}}_a$$

After transforming the above equation, we have

$$\mathbf{U}_4 = \mathbf{K}_{44}^{-1}[\bar{\mathbf{F}}_a - \mathbf{K}_{42}\mathbf{U}_2 - \mathbf{K}_{43}\mathbf{U}_3] \quad (4)$$

From the second equation of (3)

$$\mathbf{K}_{32}\mathbf{U}_2 + \mathbf{K}_{33}\mathbf{U}_3 + \mathbf{K}_{34}\mathbf{U}_4 = \mathbf{F}_c$$

\mathbf{U}_3 is computed,

$$\mathbf{U}_3 = \mathbf{K}_{33}^{-1}[\mathbf{F}_c - \mathbf{K}_{32}\mathbf{U}_2 - \mathbf{K}_{34}\mathbf{U}_4] \quad (5)$$

Substituting equation (4) into (5) gives

$$\mathbf{U}_3 = \mathbf{K}_{33}^{-1}[\mathbf{F}_c - (\mathbf{K}_{32} - \mathbf{K}_{34}\mathbf{K}_{44}^{-1}\mathbf{K}_{42})\mathbf{U}_2 - \mathbf{K}_{34}\mathbf{K}_{44}^{-1}\bar{\mathbf{F}}_a + \mathbf{K}_{34}\mathbf{K}_{44}^{-1}\mathbf{K}_{43}\mathbf{U}_3]$$

Finally, we have

$$\mathbf{U}_3 = (\mathbf{K}_{33} - \mathbf{K}_{34}\mathbf{K}_{44}^{-1}\mathbf{K}_{43})^{-1}[\mathbf{F}_c - (\mathbf{K}_{32} - \mathbf{K}_{34}\mathbf{K}_{44}^{-1}\mathbf{K}_{42})\mathbf{U}_2 - \mathbf{K}_{34}\mathbf{K}_{44}^{-1}\bar{\mathbf{F}}_a] \quad (6)$$

The first equation of (3) gives

$$\mathbf{K}_{22}\mathbf{U}_2 = \bar{\mathbf{F}}_2 - \mathbf{K}_{23}\mathbf{U}_3 - \mathbf{K}_{24}\mathbf{U}_4$$

Substituting equation (4) and (6) into the above equation, we have

$$\bar{\mathbf{K}}_{22}\mathbf{U}_2 = \bar{\mathbf{F}}_2 + \mathbf{B}_{23}\mathbf{F}_c + \mathbf{B}_{24}\bar{\mathbf{F}}_a \quad (7)$$

where

$$\bar{\mathbf{K}}_{22} = \mathbf{K}_{22} - \mathbf{K}_{24}\mathbf{K}_{44}^{-1}\mathbf{K}_{42} + (\mathbf{K}_{24}\mathbf{K}_{44}^{-1}\mathbf{K}_{43} - \mathbf{K}_{23})(\mathbf{K}_{33} - \mathbf{K}_{34}\mathbf{K}_{44}^{-1}\mathbf{K}_{43})^{-1}(\mathbf{K}_{32} - \mathbf{K}_{34}\mathbf{K}_{44}^{-1}\mathbf{K}_{42}) \quad (8)$$

$$\mathbf{B}_{23} = (\mathbf{K}_{24}\mathbf{K}_{44}^{-1}\mathbf{K}_{43} - \mathbf{K}_{23})(\mathbf{K}_{33} - \mathbf{K}_{34}\mathbf{K}_{44}^{-1}\mathbf{K}_{43})^{-1} \quad (9)$$

$$\mathbf{B}_{24} = -(\mathbf{K}_{24} + \mathbf{B}_{23}\mathbf{K}_{34})\mathbf{K}_{44}^{-1} \quad (10)$$

Solving equation (7) for \mathbf{U}_2 in term of \mathbf{F}_c gives

$$\mathbf{U}_2 = \bar{\mathbf{K}}_{22}^{-1}(\bar{\mathbf{F}}_2 + \mathbf{B}_{23}\mathbf{F}_c + \mathbf{B}_{24}\bar{\mathbf{F}}_a) \quad (11)$$

In addition, we may always find the relation between the analytical solutions of \mathbf{U}_2 and total nodal displacement vector \mathbf{U} :

$$\mathbf{U}_2 = \mathbf{A}\mathbf{U} \quad (12)$$

where \mathbf{A} is the rectangular transformation matrix which reveals the displacements at the measurement points from the complete vector of displacements.

To identify the unknown reaction or contact forces, we need to minimize the difference between the experimentally measured displacements $\bar{\mathbf{U}}_2$ and the analytical solution \mathbf{U}_2 ; therefore, we may try to calculate the L_2 -norm with respect to the identity matrix, i.e.,

$$\min_{\mathbf{F}_c} \left(\frac{1}{2} \|\bar{\mathbf{U}}_2 - \mathbf{U}_2\|_2^2 \right) \quad (13)$$

Equation (13) is equivalent to the following

$$\min_{\mathbf{F}_c} \left(\frac{1}{2} (\bar{\mathbf{U}}_2 - \mathbf{U}_2)^T \mathbf{I} (\bar{\mathbf{U}}_2 - \mathbf{U}_2) \right) \quad (14)$$

where \mathbf{I} is the identity matrix which has the same length with $\bar{\mathbf{U}}_2$.

The objective function in equation (14) is

$$\Pi = \frac{1}{2} (\bar{\mathbf{U}}_2 - \mathbf{U}_2)^T \mathbf{I} (\bar{\mathbf{U}}_2 - \mathbf{U}_2)$$

Or, after some manipulations,

$$\Pi = \frac{1}{2} (\bar{\mathbf{U}}_2^T \mathbf{I} \bar{\mathbf{U}}_2 - 2\bar{\mathbf{U}}_2^T \mathbf{I} \mathbf{U}_2 + \mathbf{U}_2^T \mathbf{I} \mathbf{U}_2) \quad (15)$$

Note that $\bar{\mathbf{U}}_2 = \bar{\mathbf{U}}_2(\mathbf{F}_c)$ is the experimental measurement displacements and $\mathbf{U}_2 = \mathbf{U}_2(\mathbf{F}_c)$ is the theoretical solution. Thus, the minimization of the objective function (15) gives, without considering any constraints,

$$\mathbf{I}\mathbf{U}_2 = \mathbf{I}\bar{\mathbf{U}}_2, \text{ or } \mathbf{U}_2 = \bar{\mathbf{U}}_2 \quad (16)$$

Substituting above equation to equation (11), we have

$$\mathbf{B}_{23}\mathbf{F}_c = \bar{\mathbf{K}}_{22}\bar{\mathbf{U}}_2 - \mathbf{B}_{24}\bar{\mathbf{F}}_a - \bar{\mathbf{F}}_2 \quad (17)$$

Note that equation (17) is a typical linear equation; \mathbf{F}_c is a vector of $n \times 1$, where n represents the number of unknown reaction or contact forces to be calculated; The right hand side of the equation is a vector of $m \times 1$, where m is the number of measured displacements; therefore, \mathbf{B}_{23} is a transformation matrix of $m \times n$. The solution of the linear equation (17) will depend on the matrix \mathbf{B}_{23} . There are three cases are found:

Case 1: $m = n$, rendering a square system. If \mathbf{B}_{23} is nonsingular (full rank), then \mathbf{F}_c is the unique solution to the linear equation. On the other hand, if \mathbf{B}_{23} is singular, the solution \mathbf{F}_c to the equation either does not exist, or is not unique.

Case 2: $m > n$, over-determined system. If the rank of the rectangular matrix \mathbf{B}_{23} is n , then \mathbf{F}_c is the solution in the least squares sense to the over-determined system of equation. And \mathbf{F}_c is the unique solution to the linear equation. Rectangular matrix \mathbf{B}_{23} is rank deficient (rank $< n$) if it does not have linearly independent columns. If \mathbf{B}_{23} is rank deficient, the least square solution to the equation is not unique.

Case 3: $m < n$, underdetermined system. Underdetermined linear systems involve more unknowns than equations. It means there are more unknown forces need to be identified than the number of measurements. In this case, the solution \mathbf{F}_c is never unique. We may find a basic solution using MATLAB [16], which has at most m nonzero components, but even this may not be unique.

3. Tikhonov-Phillips Regularization Method

Considering the measured error may exist in the displacements \mathbf{U}_2 , Tikhonov-Phillips regularization technique is employed to reduce the influence of the measurement noise. Let the objective function be

$$\Pi^* = \frac{1}{2} \|\mathbf{U}_2 - \bar{\mathbf{U}}_2\|_{\mathbf{B}}^2 + \frac{1}{2} \lambda \|\mathbf{F}_c\|^2 \quad (18)$$

where

$$\|\mathbf{X}\|_{\mathbf{B}}^2 = \mathbf{X}^T \mathbf{B} \mathbf{X}, \text{ and } \|\mathbf{X}\|^2 = \mathbf{X}^T \mathbf{X}$$

Further, λ is a conditional number and \mathbf{B} is an arbitrary matrix to be chosen later. Therefore,

$$\Pi^* = \frac{1}{2} (\mathbf{U}_2 - \bar{\mathbf{U}}_2)^T \mathbf{B} (\mathbf{U}_2 - \bar{\mathbf{U}}_2) + \frac{1}{2} \lambda \mathbf{F}_c^T \mathbf{F}_c \quad (19)$$

The minimization of the above objective function is

$$\min_{\mathbf{F}_c} \left[\frac{1}{2} (\mathbf{U}_2 - \bar{\mathbf{U}}_2)^T \mathbf{B} (\mathbf{U}_2 - \bar{\mathbf{U}}_2) + \frac{1}{2} \lambda \mathbf{F}_c^T \mathbf{F}_c \right] \quad (20)$$

Thus,

$$(\mathbf{U}_2 - \bar{\mathbf{U}}_2)^T \mathbf{B} \frac{\partial \mathbf{U}_2}{\partial \mathbf{F}_c} + \lambda \mathbf{F}_c^T = 0 \quad (21)$$

Differencing Eqn. (7) with respect to \mathbf{F}_c , we have

$$\bar{\mathbf{K}}_{22} \frac{\partial \mathbf{U}_2}{\partial \mathbf{F}_c} = \mathbf{B}_{23} \quad (22)$$

Therefore, if we choose $\mathbf{B} = \bar{\mathbf{K}}_{22}$, equation (21) becomes

$$(\mathbf{U}_2 - \bar{\mathbf{U}}_2)^T \mathbf{B}_{23} + \lambda \mathbf{F}_c^T = 0 \quad (23)$$

Notice that \mathbf{B}_{23} can be calculated using equation (9), it shows that the partial differential equation (21) is simplified to a linear algebra equation after choosing a proper \mathbf{B} , which making the problem much easier to be solved. Taking the transpose of the above equation:

$$\mathbf{B}_{23}^T \mathbf{U}_2 + \lambda \mathbf{F}_c = \mathbf{B}_{23}^T \bar{\mathbf{U}}_2 \quad (24)$$

Substituting equation (11) into the above, we have

$$\mathbf{B}_{23}^T \bar{\mathbf{K}}_{22}^{-1} \mathbf{B}_{24} \bar{\mathbf{F}}_a + \mathbf{B}_{23}^T \bar{\mathbf{K}}_{22}^{-1} \mathbf{B}_{23} \mathbf{F}_c + \lambda \mathbf{F}_c + \mathbf{B}_{23}^T \bar{\mathbf{K}}_{22}^{-1} \bar{\mathbf{F}}_2 = \mathbf{B}_{23}^T \bar{\mathbf{U}}_2 \quad (25)$$

Therefore,

$$(\mathbf{B}_{23}^T \bar{\mathbf{K}}_{22}^{-1} \mathbf{B}_{23} + \lambda \mathbf{I}) \mathbf{F}_c = \mathbf{B}_{23}^T (\bar{\mathbf{U}}_2 - \bar{\mathbf{K}}_{22}^{-1} \mathbf{B}_{24} \bar{\mathbf{F}}_a - \bar{\mathbf{K}}_{22}^{-1} \bar{\mathbf{F}}_2) \quad (26)$$

Note that:

1. If $\lambda = 0$, equation (26) returns to equation (17).
2. We always assume that the operator $\mathbf{B}_{23}^T \bar{\mathbf{K}}_{22}^{-1} \mathbf{B}_{23} + \lambda \mathbf{I}$ is boundary invertible according to Theorem 2.12 in [20]; therefore, equation (26) should have the unique solution by providing a proper conditioning number λ .

4. Application Examples

Three examples are selected to demonstrate the accuracy of the present method. To demonstrate the current inverse algorithm, the first example selected is to identify the known applied forces, which is assuming unknown in the inverse algorithm. For comparison, last example selected is of Hertzian problems, whose analytic solutions can be found in the literature.

In the first example shown in Figure 2, a planar uniform cantilever beam subjected to four constant nodal forces. The cross-section of the beam is 1in. by 1in, resulting in a moment of inertia is $1/12 \text{ in}^4$, the elastic modulus is 10^7 psi . The constraints are applied to the left boundary support point (fixed boundary condition), i.e. $v_1 = 0, \theta_1 = 0$.

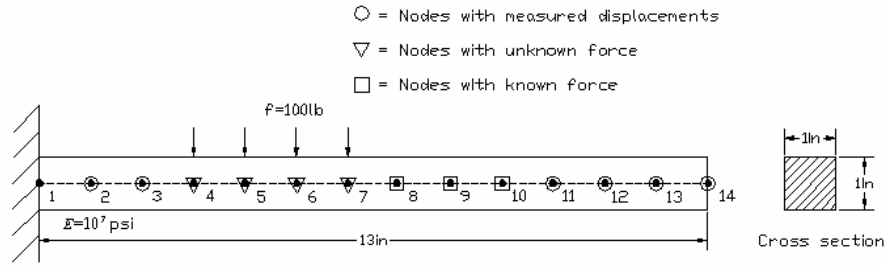


Figure 2. Cantilever beam finite element model with constant nodal load $f = 100 \text{ lb}$ at node 4, 5, 6, and 7.

According to the known boundary conditions and applied forces, a direct FEM solution of this model was used to solve for the displacements and slopes at nodes 2, 3, 11, 12, 13 and 14. In the inverse problem, we assume the applied forces are unknown, use the displacements at node 2, 3, 11, 12, 13 and 14 as known measurements to back calculate the applied loads followed the proposed inverse procedure. The inverse solution is shown in Table 1. The results show that the inverse solution of the nodal forces at node 4, 5, 6 and 7 are exactly to the applied nodal forces on the nodes. Therefore, the applied forces can be quantified accurately if there is no error in the measurements.

Table 1. A comparison of the regularized inverse solution of applied forces for a cantilever beam with actual applied force. Unit of force is lb

Node #	N4	N5	N6	N7
Applied force	-100	-100	-100	-100
Inverse solution	-100	-100	-100	-100
Inverse solution with 1% measured error	-0.8882×10^5	3.0346×10^5	-3.5752×10^5	1.4539×10^5
Regularized solution	-91.72	-92.05	-100.23	-105.93
Error (%)	8.28	7.95	0.23	5.93

To simulate the practical measurements, a uniform distributed random error of 1% was added to the “measured” displacements at node 2, 3, 11, 12, 13 and 14 as the simulated data. And the simulated data were used to calculate the nodal forces. When the “measured” error is between plus and minus 1 percent, it is found that the calculated nodal forces without regularization are too far from the actually applied load. Therefore, this is an ill-posed problem.

To acquire a useful and stable solution, two regularization techniques were used. In the Tikhonov-Phillips regularization method, when regularization parameter λ was chosen 3.1623×10^{-7} , and the regularized solution of the nodal forces are listed in Table 1. It is readily seen that the regularized solution provides a good approximate to the expected values.

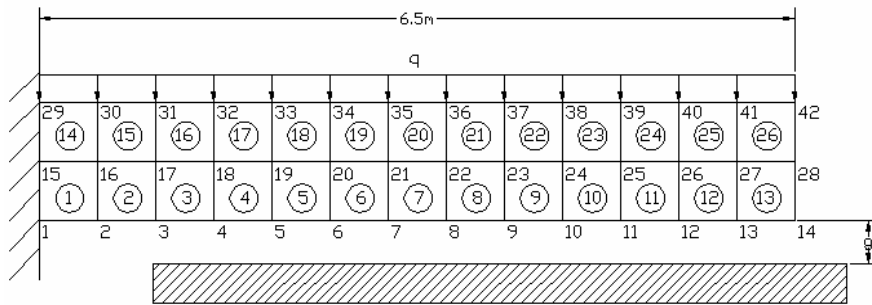


Figure 3. Finite element model of a cantilever beam contacting rigid ground using isoparametric plane stress elements. Uniformly distributed load $q = 1000 \text{ N/m}^2$, gap size $g = 0.1 \text{ m}$.

The second example is a cantilever beam bent to a rigid plane by a uniformly distributed load. The beam is modeled using two-dimensional isoparametric elements assuming plane stress condition. The finite element model is shown in Figure 3, in which 26 quadrilateral elements are used. Each node has two degrees of freedom (u, v). The beam has an elastic modulus of 10^6 N/mm^2 , and a length of 6.5 m. The left end of the beam is fixed; the initial gap between the bottom surface of the beam and the rigid ground is 0.1 m. A distributed load of q is applied on the top of the beam. Following the same procedures used in the first example, direct problem is first solved to generate displacements for simulating the measurements. For example, the vertical displacements on the top of the beam can be treated as the measured data (simulated from direct method). Those data (which play the role of experimental

measurements) are used together with the proposed inverse algorithm to calculate the contact forces between the beam and rigid surface.

The contact forces and contact area calculated above are based on the noise free measurements. However, the measured error is sometimes unavoidable. Therefore, we have to consider the influence of the measurement error on the result. Assuming the distributed load is 1000 N/m^2 , the calculated displacements from the direct method (the noise-free measured displacements) are plot in Figure 4. To simulate the real measurements, a random error was added to the calculated displacements. Those inexact data (which play the role of experimental measurements) were used together with the proposed inverse algorithm to calculate the contact forces between the beam and rigid surface.

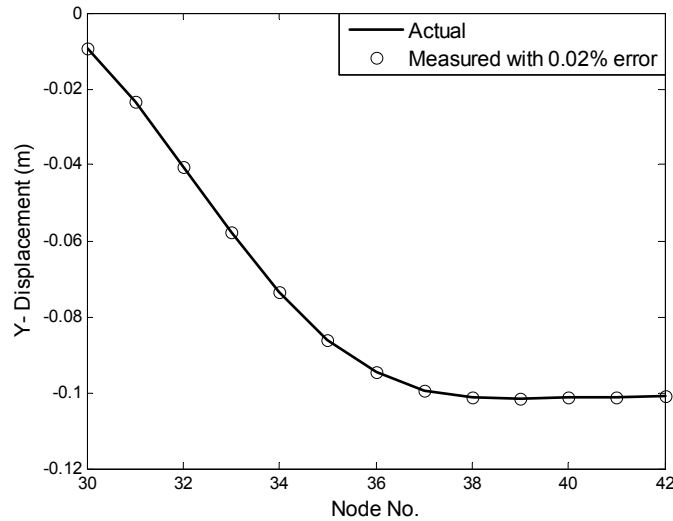


Figure 4. Simulation of measurements from the direct solution of the top surface of the cantilever beam.

The solution was found to diverge rapidly when only a least square method was used without any regularization. This is due to the ill-posed of the inverse problem. Once again, Tikhonov-Phillips regularization method is used. The resulting contact forces and nodal displacements in the contact zone are shown in Figure 5 and Figure 6, respectively. It was found that the regularization method does reduce the influence of the measurement error and produce a good approximation of the solution.

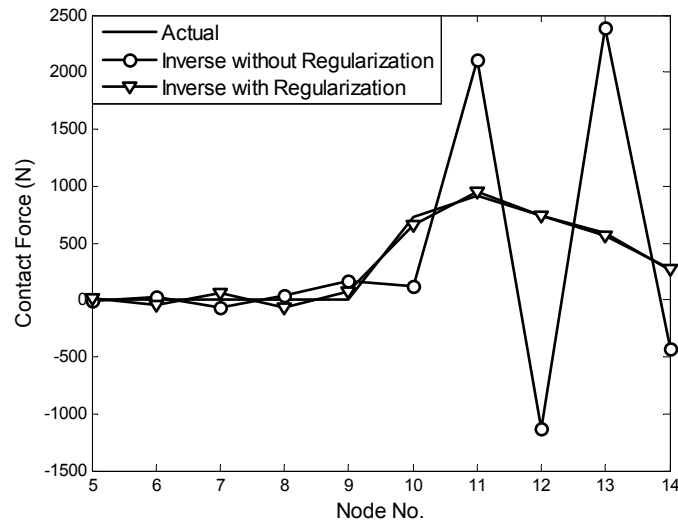


Figure 5. Contact forces calculated from inverse algorithm with/without regularization and the direct solution.

Table 2 shows the comparison of the results from the inverse algorithm and ANSYS. It is readily seen that the results are in excellent agreement.

The third example shown in Figure 7(a) is the elastic contact between a long cylinder with a radius of 50mm and a plane surface of the rigid half space, for which an analytical solution is available. The finite element mesh shown in Figure 7(b) represents a half of the cross-section of the cylinder modeled as a plane strain problem. The rigid plane is modeled by a rigid element that is fixed in

space. The following parameters are chosen for the problem: Young's modulus $E = 103 \text{ N/mm}^2$, Poisson's ratio $\nu = 0.3$ and a half load of $F = 55 \text{ N}$. The two-dimensional model has 147 four-node quadrilateral elements and 174 nodes each with two translational degrees-of-freedom.

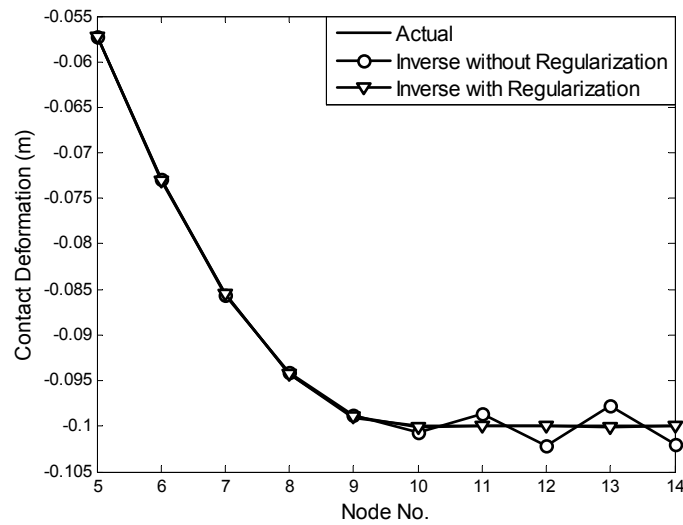


Figure 6. Contact deformation from inverse algorithm with/without regularization and the direct solution.

Table 2. A comparison of the contact forces from the inverse method and the commercial finite element package ANSYS using isoparametric plane stress elements. Unit for force is N.

NODE	ANSYS	Inverse FEA	Error	Error %
9	0.00	0.01	-0.01	N/A
10	915.47	915.39	0.08	0.01%
11	911.22	911.25	-0.03	0.00%
12	686.52	686.50	0.02	0.00%
13	543.40	543.42	-0.02	0.00%
14	242.11	242.08	0.03	0.01%

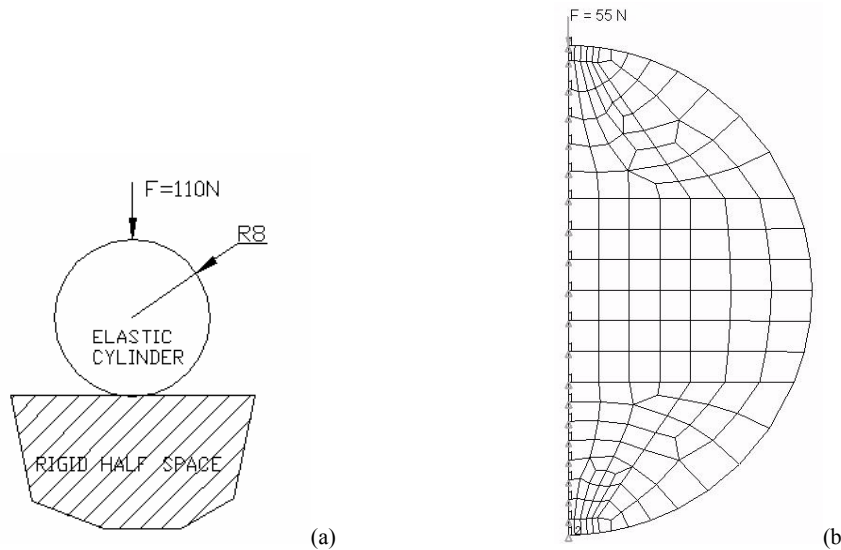


Figure 7. (a) Contact between an elastic long cylinder and the rigid half space. Unit: mm; (b) A half finite element model of the cross-section of the cylinder modeled as a plane strain problem.

The calculated nodal contact force using the current inverse algorithm is shown in Figure 8, in which the Hertzian solution and ANSYS solution are also shown. It can be seen that the current inverse FEA solutions, contact radius and contact forces, are almost identical to the ANSYS solutions. The radius of contacting area from the current inverse algorithm is 1.02 mm as compared with 1.01 mm by the Hertzian solution. In addition, the contact forces from the inverse algorithm are a little bit higher but very close to the

Hertzian solution. Table 3 summarizes the nodal contact forces in contact zone calculated by three different methods. We see that good agreement (less than 6 percent error) between the inverse FEA solution and the Hertzian and the commercial FE code ANSYS except the last node.

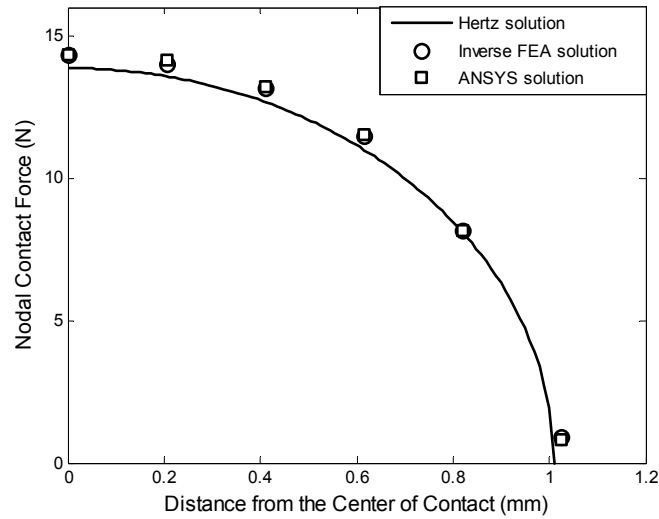


Figure 8. Comparison of the contact force calculated from inverse algorithm, ANSYS commercial finite element package with the exact Hertz solution.

It should be pointed out that the agreement of the inverse FEA solution with the Hertzian solution is changing at different load levels and with different finite element mesh. When the load level is such that the contacting area terminates at a node, the inverse FEA solution and Hertzian solution agree well. If the contacting area terminates somewhere between two finite element nodes, the errors will be introduced to the results of extracted contact forces and contact area. However, it is believed that such errors can be reduced if the finite element mesh is refined.

Figure 9 shows possible errors in calculation of contact forces and contact area for a two-dimensional case. As shown in Figure 9 (a), the contacting area terminates between node 2 and node 3. By assuming a linear distribution of contact pressure over a complete contact segment, we have to assume either no pressure between node 2 and node 3 (case 1) as shown in Figure 9 (b) or a linear pressure distribution between the two nodes (case 2) as shown in Figure 9 (c). In case 1, the contact area terminates at node 2 that underestimates the contact area ($r_1 < r$). As to the contact pressure, since the contact between node 2 and node 3 is ignored, therefore, the contact pressure is also underestimated. Similarly, in case 2, the contact area terminates at node 3 that overestimates the contact area ($r_2 > r$). In addition, the contact pressure between node 2 and node 3 is also overestimated. In contact problems, these errors are sometimes unavoidable if the contact area is not known *a priori*. However, it is believed that the error can be reduced through refining the mesh on the boundary separating the contact and non-contact regions [21].

Table 3. A comparison of the nodal contact force calculated from inverse algorithm, ANSYS commercial finite element package with the exact Hertz solution. Unit for force is N.

NODE	ANSYS	Exact	Inverse FEA	Error	Error %
7	7.1770	7.1036	7.1680	-0.0644	0.9%
8	14.1300	13.9050	14.0278	-0.1228	0.9%
9	13.1980	12.9567	13.1805	-0.2238	1.7%
10	11.5370	11.2060	11.4823	-0.2763	2.5%
11	8.1512	8.1454	8.1397	0.0057	0.1%
12	0.8068	0	0.9175	0.7658	N/A

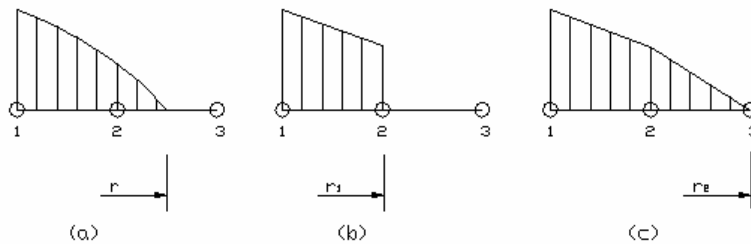


Figure 9. Possible errors in calculation of contact forces and contact area.

5. Conclusion

In this paper, we have developed an inverse algorithm to solve the contact forces and contact deformation using the measured displacements. The unknown loads or contact forces are identified by minimizing an objective function derived as the L_2 -norm of the differences between the measurements and the numerical results from the finite element method. A detail description of the formulation, analysis and solution of the inverse problems are given in the presentation. Tikhonov-Phillips regularization technique is employed to reduce the influence of the measurement noise. Three testing examples are chosen to demonstrate the accuracy of the numerical scheme. In the first example involving a beam problem, good agreement between the regularized inverse solution and the known applied forces is achieved. The second example shows the contact forces and deformation shape of 2D elastic beam subjected to four different uniform distributed loads, excellent agreement between regularized inverse solution and the commercial FE code ANSYS. The third example is investigated a Hertz contact problem between a long cylinder and a plane surface of the rigid half space. A good agreement is found for both the contact forces and contact radius to the exact Hertz solution. Furthermore, the possible reason for a significant difference existing in the contact force close to the contact boundary is addressed, which accounts for a larger contact radius in our FEA model. The analysis results reveal that the present inverse method is accurate and efficient. Although the simple examples are analysis in this paper, the developed inverse algorithm can be extended to the more complicated geometries and contact problems. And it is anticipated that the present technique can be used to predict the contact forces, contact radius and deformed configurations of the objects.

Acknowledgement

The second author appreciates the partial support from the Fastening and Joining Research Institute, Oakland University, administered by Director Dr. Sayed Nassar.

References

1. ANSYS user's manual, revision 6.1, Canonsburg, PA, ANSYS Inc.
2. ABAQUS user's manual, version 6.3, Pawtucket, RI, Hibbitt, Karlsson & Sorensen, Inc.
3. H. Hertz, On the contact of elastic solids, *J. Reine Angew. Math.* 92 (1881), pp. 156-171.
4. R.D. Cook, D.S. Malkus, and M.E. Plesha, *Concept and Applications of Finite Element Analysis*, 3rd ed., New York: John Wiley, 1989.
5. R.J. Gu, P. Murty, and Q. Zheng, Use of penalty variable in finite element analysis of contacting objects, *Compu. & Struc.* 80 (2002), pp. 2449-2459.
6. L.T. Campos, J.T. Oden, and N. Kikuchi, Analysis of a class of contact problems with friction in elastostatics, *Comput. Meth. Appl. Mech. Eng.* 34 (1982), pp. 821-845.
7. J.T. Oden, and N. Kikuchi, Finite element methods for constrained problems in elasticity, *Int. J. Numer. Meth. Eng.* 18 (1982), pp. 701-725.
8. G. Yagawa, and H. Yagawa, A finite element method for contact problems related to fracture mechanics, *Int. J. Numer. Meth. Eng.* 20 (1984), pp. 2175-2195.
9. W.H. Chen, and P. Tsai, Finite element analysis of elastodynamic sliding contact problems with friction, *Comput. Struct.* 22 (1989), pp. 925-938.
10. K.J. Bathe, and A. Chaudhary, A solution method for planar and axisymmetric contact problems, *Int. J. Numer. Meth. Eng.* 21 (1985), pp. 65-88.
11. R.J. Gu, Moving finite element analysis for elastic beams in contact problems, *Comput. Struct.* 24 (1986), pp. 571-579.
12. R.J. Gu, Moving finite element analysis for indentation of elastic beams, *Finite Elem. Anal. Des.* 4 (1988), pp. 267-278.
13. R.J. Gu, Moving finite element analysis for two-dimensional frictionless contact problems, *Comput. Struct.* 33 (1989), pp. 543-549.
14. J.P. Fuehne, and J.J. Engblom, Finite element/penalty function method for computing stresses near debonds, *AIAA J.* 30 (1992), pp. 1625-1631.
15. N. El-Abbasi, and K.J. Bathe, Stability and patch test performance of contact discretizations and a new solution algorithm, *Comput. Struct.* 79 (2001), pp. 1473-1486.
16. Matlab document, Version 6.1 Release 12.1, The MathWorks, Inc, 2001.
17. R.J. Gu, and G.C. Barber, Determination of true dimensional quality and build errors using coordinate measurement data, *ASME J. Manu. Sci. Eng.* Vol. 121 (1999), pp. 749-755.
18. M. Bonnet, and A. Constantinescu, Inverse problems in elasticity, *Inver. Prob.* 21 (2005), pp. 1-50.
19. R.J. Gu, Reconstruction of contact pressures between flexible objects and rigid planes using friction data, *Applied Math. Modelling*, V.19, N.10, pp. 578-582, Oct. 1995.
20. A.N. Tikhonov, and A.V. Arsenin, *Solutions of Ill-Posed Problems*, Winston, Washington, D.C., 1977.
21. Z.H. Zhong, *Finite element procedures for contact-impact problems*, Oxford Science Publications, New York, 1993.